Subproject B2.7

Experimental Investigation of Electron Transport in Hybrid Nanostructures

Principle Investigators: Hilbert v. Löhneysen, Christoph Sürgers, Detlef Beckmann

CFN-Financed Scientists: Alexander Cosceev (BAT IIa, 6 months), Michael Marz (71% BAT IIa, 36 months), Heiko Stalzer (BAT IIa, 6 months), Niraj Joshi (BAT IIa, 12 months), Marc Müller (5/8 BAT IIa, 6 months), Oliver Berg (1/2 BAT IIa, 5,5 months), Sebastian Zaum (3/4 BAT IIa, 3 months)

Further Scientists: Florian Hübler (IFP), Gernot Goll (PI), Markus Stokmaier (PI)

Physikalisches Institut
KIT – Campus Süd

Institut für Nanotechnologie
KIT – Campus Nord

Experimental Investigation of Electron Transport in Hybrid Nanostructures

Introduction and Summary

In this subproject we investigate the electronic transport in metallic nanostructures comprised of different materials with competing electronic interactions. The focus is on superconductor/ferromagnet hybrid structures which are studied by means of electrical resistance measurements (local and nonlocal) in dependence of temperature, magnetic field, and applied voltage. These measurements allow to explore the effect of ferromagnetic order and the spin splitting of the electron conduction bands on the superconducting properties.

The proximity effect between a superconductor S in contact with a normal metal N or a ferromagnet F has been intensively studied in the last decade. However, little has been known about the magnetic response of S/N double layers. We have determined the diamagnetic response of Nb/Ag and Nb/Ag/Fe layers. While the former exhibits a clear diamagnetic signal of proximity-induced superconductivity (PIS) in Ag (in addition to the expected signal from Nb), this signal is quenched for the latter when the Ag thickness is d_{Ag} = 550 nm. Surprisingly, diamagnetic screening reappears in Nb/Ag/Fe layers for small d_{Ag} = 40 nm. This behavior can be understood in terms of a delicate balance between PIS and pairbreaking by F.

The transition temperature T_c of a superconductor sandwiched between two F layers depends on the relative magnetization orientation of the latter with respect to each other, parallel (P) or antiparallel (AP). Both positive and negative $\Delta T_c = T_c^P - T_c^{AP}$ have been investigated. We have for the first time reralized this superconducting spin-valve (SSV) effect for sandwiches with out-of-plane magnetizations employing Co/Pt multilayers with different coercive fields for the two F layers. The observed *positive* ΔT_c is attributed to the diffusion and scattering of non-equilibrium spin-polarized charge carriers.

The spin-sensitivity of Andreev reflection through an S/F nanocontact can be employed to determine the spin polarization P of the current. We have found that P depends on the diameter of the S/F contact and approaches the bulk (equilibrium) value for small contacts. The apparent reduction of P for larger contacts has been attributed to spin-orbit interaction.

Non-local transport in hybrid structures can be investigated in multiterminal devices. In particular, non-local Andreev reflection is possible if the injector (I) and detector (D) contacts are placed within the superconductive coherence length as we demonstrated for the first time. We have investigated in detail the conductance due to non-local Andreev reflection and electron co-tunneling, which depends on the bias applied to I and D in a complex fashion probably caused by quantum-mechanical interference.

In the course of experiments to determine the role of random magnetic fields on weak localization in Pd films we chose the dilute ferromagnet $Eu_xSr_{1-x}S$ as a substrate to provide the random fields. We surprisingly found superconductivity in very thin Pd films of 7 nm thickness. We could infer from the monotonic T_c decrease with increasing Eu concentration x of the substrate attributed to pair breaking that superconductivity in Pd is of conventional s-wave character. Furthermore, the analysis of $T_c(x)$ led to a detailed characterization of the pair-breaking mechanism. Field-effect and Hall-effect measurements suggest that superconductivity is caused by charge transfer at the interface.

1. Diamagnetic Screening in Superconductor/Ferromagnet Multilayers

The proximity effect in multilayers (ML) of a superconductor (S) in contact with a normal metal (N) or a ferromagnet (F) has been intensely studied during the past decade. In S/F contacts with strong ferromagnets the pair-condensate amplitude decays on a length scale of the order of the electron mean free path l_F in F [B2.7:5,1]. In S/N systems the diamagnetic transition of the N layer shifts to higher temperatures with decreasing d_N indicating an enhanced stability of the proximity-induced superconductivity (PIS) [B2.7:2], whereas the cladding of the outer N surface by a ferromagnetic metal gives rise to additional pair breaking. Little is known about the magnetic response of clean S/N double layers with thickness d_N in the submicrometer range where N is in contact with F. In S/N/F systems with appropriate N layer thickness, a concurrent influence of PIS and pair breaking by F on N should be observed, as was demonstrated in this project.
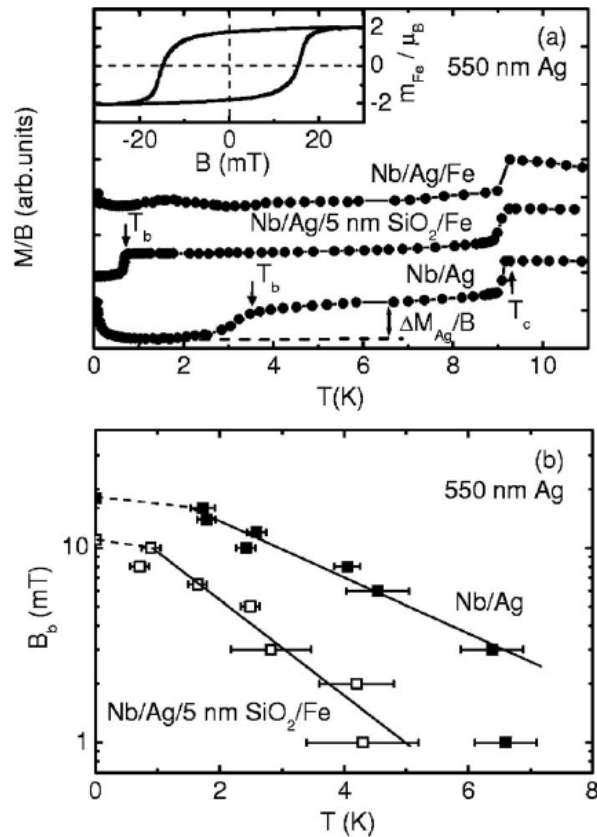

Fig. 1: (a) $M(T/B)$ for samples with d_{Ag} = 550 nm and d_{Fe} = 40 nm in a field of B = 8 mT. T_c and T_b indicate the diamagnetic transition of the Nb and Ag layers, respectively. Inset shows the magnetization curve of the Nb/Ag/Fe sample taken at T = 10 K. (b) Semilogarithmic plot of $B_b(T)$. Solid lines indicate a behavior $\ln B_b \sim T/T_A$. Dashed lines serve as guides to the eye toward $B_b(0)$. From Ref. [B2.7:8].

We performed magnetization measurements on high-quality Nb/Ag double layers and Nb/Ag/Fe multilayers with 200 nm Nb, d_{Ag} < 1 m, and 40 nm Fe [B2.7:2, B2.7:8, B2.7:10]. The magnetization M at constant B applied parallel to the sample surface was measured as a function of T in a coaxial dB_z/dz gradiometer coupled to a SQUID. Figure 1(a) shows $M(T)/B$ of a Nb/Ag double layer with d_{Ag} = 550 nm. The sharp diamagnetic signal at T_c = 9.1 K is due to the superconducting transition of the Nb layer. At a lower temperature T_b, a further diamagnetic transition of height M_{Ag}/B occurs which is attributed to the proximity-induced diamagnetic

screening currents in the Ag layer. The temperature dependence of the critical field $B_b(T)$ in Fig. 1(b) and the characteristic temperature T_A obtained from the slope of $B_b(T)$ is in good agreement with thermodynamic calculations for the clean limit [2].

Deposition of a 40 nm thick Fe layer directly onto Ag with d_{Ag} = 550 nm suppresses the diamagnetic signal down to below the lowest temperature of 60 mK, see Fig. 1(a). The Andreev pairs, penetrating into the ferromagnetic layer from the "normal conducting" N, experience an additional phase shift in Fe, which destroys the phase coherence in Ag. For a sample with a 5-nm thick insulating SiO2 layer between Ag and Fe the influence of the Fe layer is considerably weakened and a diamagnetic signal of Ag reappears but at a much lower T_b when compared to the Nb/Ag double layer. The Andreev pairs have a finite probability to tunnel into Fe via SiO2 and back again, so that their phase coherence is compromised by the exchange interaction I_{ex} of Fe. In other words, for a fixed temperature, smaller external fields are sufficient for the destruction of coherence in comparison with Nb/Ag double layers.

Surprisingly, diamagnetic screening of Ag *without* a SiO2 barrier reappears in Nb/Ag/Fe samples with much smaller d_{Ag}= 35 and 43 nm in a certain range of magnetic field. Fig. 2 clearly shows transitions around 3 K, which shift only slightly to lower temperatures with increasing field B together with an increase of the jump M_{Ag}/B. The result can qualitatively explained in the following way. For d_{Ag} = 35 and 43 nm, the Andreev energy corresponds to T_A = 48 and 39 K >> T_c, respectively, so that the coherence in the Ag layer will not be destroyed in contact with the ferromagnetic Fe layer. The magnitude of the diamagnetic signal is also determined by the density of Andreev pairs. Roughly speaking, the PIS in Ag is stabilized for thinner d_{Ag} (higher T_A) but at the same time, it is weakened by the pair breaking due to the contact with Fe. The balance between these effects can lead to the observation of a diamagnetic transition in Ag for certain d_{Ag} and B.
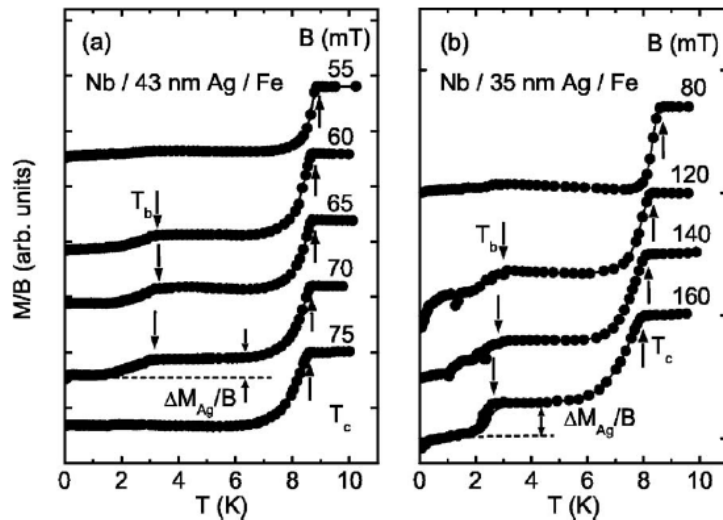

Fig. 2: $M(T)/B$ of Nb/Ag/Fe samples with d_{Fe} = 40 nm for different d_{Ag} and fields B. From Ref. [B2.7:8]

2. Superconductor / Ferromagnet Spin Valves with Perpendicular Magnetic Anisotropy

In an all-metal F/S/F superconducting spin valve (SSV) the superconducting transition temperature T_c of an S layer sandwiched between two F layers depends on the relative orientation of the two in-plane magnetizations, parallel (P) or antiparallel (AP) [3]. The two magnetic configurations P and

AP of the SSV can be achieved even in zero magnetic field when tailoring different coercive fields of the two F layers. In the frame of the proximity-effect theory, the difference in T_c is explained by the fact that the Cooper pair samples the direction of the different exchange fields (due to relative orientation of the F layers) within its coherence volume [1,3]. The first experimental realization of such an all-metal SSV effect was reported by Gu *et al.* [4]. However, inhomogeneous magnetic stray fields arising from a multidomain structure can also affect T_c of the S layer and can mimic a SSV behavior in F/S/F systems [5]. Besides the proximity effect due to AR considered so far, the spin-dependent scattering at S/N or S/F interfaces has to be taken into account. A GMR effect was observed in oxide S/F-ML [6]. The GMR-like mechanism will result in a reduction of the superconductive energy gap Δ due to the enhanced number of spin-polarized quasiparticles in S, provided that the thickness of superconductor is shorter than the spin diffusion length l_{sf}.

In F/S/F multilayers with magnetic out-of-plane anisotropy, different magnetic states - magnetized or demagnetized - can be achieved for the individual F layers by appropriate choice of the applied magnetic field [7]. In Ref. [B2.7:7, B2.7:9, B2.7:11] we have studied the dependence of the superconducting transition temperature T_c on the magnetization orientation in $[Co/Pt]^b/Nb/[Co/Pt]^t$ triple layers, where a Nb film is squeezed between a bottom (b) and top (t) Co/Pt-ML with high perpendicular magnetic anisotropy. The magnetization curve $M(H)$ for the F/S/F sample with $d_{Nb} = 200$ Å, measured in a vibrating sample magnetometer (VSM) above T_c with the magnetic field oriented perpendicularly to the sample plane, is shown in Fig. 3(a). The hysteresis loop is characteristic for two ferromagnetic films with perpendicular magnetic anisotropy and with different coercive fields due to the different substrate temperatures during growth. As a result of the difference (≈ 190 mT) in coercive field, the P configuration can be easily achieved by increasing the field to 1 T just above T_c and subsequently reducing the field to zero. In order to obtain the AP configuration, a field of -350 mT was applied just above T_c and after that the field is reduced to zero, see the half loop in Fig. 3(a). In this case the remanent magnetization is zero.
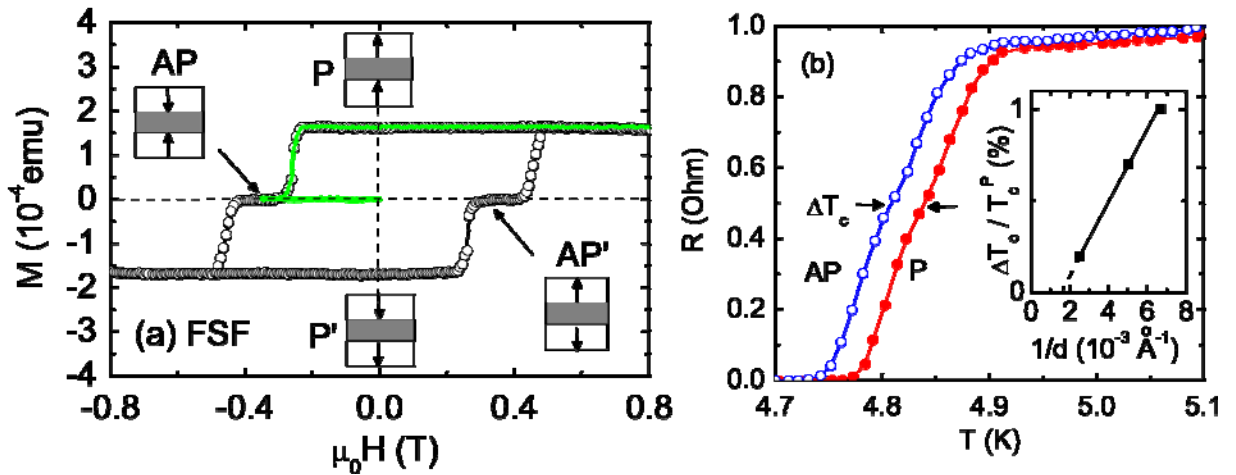

Fig. 3: (a) Hysteresis loop (open symbols) *M* vs. *H* at *T* = 8 K of an F/S/F sample with
$d_{Nb} = 200$ Å, Nb ($T_c = 4.835 \pm 0.002$ K). The different parallel (P, P') or antiparallel (AP, AP') magnetic configurations are schematically indicated (grey area: Nb) and the green curve shows a half loop. (b) Resistance *R* vs. temperature *T* in the P and AP configuration of both F layers. Inset shows a dependence $\Delta T_c / T_c^P \sim 1/d_{Nb}$ for the different F/S/F samples. From Ref. [B2.7:11].

The electrical resistance R vs. temperature T was measured by the standard four-probe method with the current in the plane (CIP). The resistively measured superconducting transitions are shown in Fig. 3(b). T_c is higher for the P than for the AP configuarion with a difference of $\Delta T_c = T_c^P - T_c^{AP} = 32$ mK. The relative T_c difference $\Delta T_c / T_c^P$ increases with decreasing Nb thickness and is large when the Nb thickness is of the order of the Ginzburg-Landau coherence length $\xi_{GL}(0)$ estimated to 160 Å from the temperature dependence of upper critical field H_{c2} (T) (not shown). These results are in contrast to some previous results obtained for F/S/F triple layers with in-plane magnetization [4,8] but were also observed for some sputtered F/S/F triple layers [9] and oxide hybrids [6], where the different states were likewise obtained by different coercive fields and not by using an antiferromagnetic layer for exchange bias.

The observed difference in T_c might possibly be caused by different stray fields of the top and bottom F layer. However, *M(H)* has a horizontal slope when crossing *M(H=0)*, with a remanent magnetization being equal to the saturation magnetization. Moreover, the temperature dependence of the upper critical field of our samples shows a linear behavior for both P and AP states (not shown) in contrast to the anomalous behavior observed for F/S/F samples with perpendicular anisotropy in the presence of stray fields [7]. Furthermore, the stray field of the perpendicularly magnetized F films is close to zero (except at the sample edges) [7] in agreement with the fact that a homogeneous thin film magnetized perpendicularly does not exhibit a magnetic stray field. Indeed, a low-temperature study by magnetic force microscopy (MFM) on our samples [B2.7:7] did not show domain walls in the MFM images acquired for the P and AP states confirming that no stray fields exist in these states (well away from the edges of the sample).

The interpretation that the experimental result $T_c^P > T_c^{AP}$ arises from an enhanced backscattering of spin-polarized charge carriers at the F/S interface into S for the AP case is corroborated by investigating F/I/S/I/F samples, where insulating (I) SiO_2 films of 25 Å thickness were introduced between the F and S layers to suppress the transmission of charge carriers between the individual layers. In this case, the strong increase of T_c^P compared to the corresponding F/S/F sample clearly demonstrates that in this case the proximity effect is indeed suppressed. More importantly, T_c^P is independent of the magnetic configuration of the F layers.
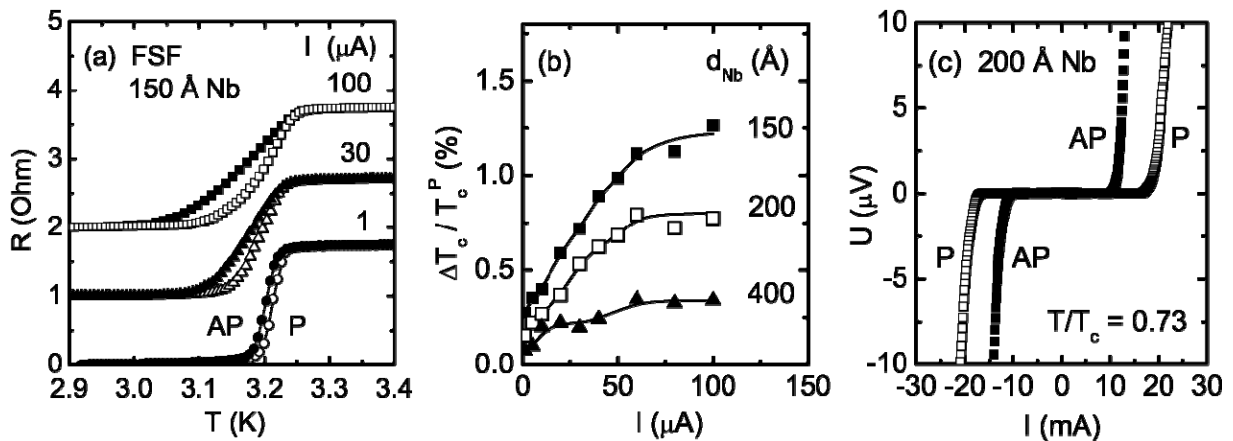

Fig. 4: (a) Resistive superconducting transitions for an F/S/F triple layer in the AP state (closed symbols) and P state (open symbols) for different in-plane currents *I*. Each curve is shifted upward by 1 Ohm for clarity. (b) The relative T_c difference $\Delta T_c / T_c^P$ vs. current *I* for different d_{Nb}. (c)Voltage-current characteristics at $T/T_c = 0.73$. From Ref. [B2.7:7].

If spin-dependent scattering plays a dominant role, the difference $\Delta T_c / T_c^P$ should increase with increasing current, i.e., with increasing number of spin-polarized quasiparticles injected from F into S. This picture is also valid for the CIP configuration used here, where only a fraction of the charge carriers will cross the interfaces between the S and F layer. Fig. 4(a) shows the effect of the transport current I on the $R(T)$ behavior. The main result is that the difference between the Tc values in the P and AP states increases with current I (or current density J). This is in agreement with the assumption that the transport current induces a diffusion of non-equilibrium spin-polarized charge carriers from F to S, thus reducing T_c. Fig. 4(b) shows that the relative T_c difference increases almost linearly with I for small I and eventually saturates. Fig. 4(b) further shows that for a fixed current I the magnitude of $\Delta T_c / T_c^P$ increases with decreasing Nb thickness, indicating that the spin-polarized charge carriers are effective in breaking of Cooper pairs only within the spin-diffusion length $l_{sd} \approx 250$ Å. An interesting detail is the finite offset of ΔT_c for $I \rightarrow 0$, i.e., $T_c^P > T_c^{AP}$ is still observed under near-equilibrium conditions in contrast to the explanation by the proximity effect. The superconducting critical current also depends on the magnetic state and is somewhat higher for the P state than for the AP state as shown in Fig. 4(c). This again proves the existence of a true AP state with saturated F layers, because a multi-domain state would give rise to an increased pinning of induced vortices and therefore to a higher critical current in the AP state contrary to what is observed.

For a detailed investigation of the spin-polarized transport through F/S/F hybrids and comparison with theory [10], measurements in current-perpendicular-to-plane (CPP) geometry are required. This can be achieved by preparing nanostructured samples using shadow-mask evaporation [11]. We have started the fabrication of such hybrid structures by using of a layout of the Si_3N_4 mask that allows four-point measurements of the resistance of [Co/Pt]/Nb/[Co/Pt] samples (Fig. 5). Preliminary measurements of the transition temperature shows that T_c is higher in the AP state compared to the P state (Fig. 5). This is in contrast to our previous results obtained in the CIP configuration as well as to what is expected from the spin-dependent transport. However, the resistance well below and above T_c is ≈ 0.2 Ohm higher in the AP state compared to the P state in agreement with the GMR effect. This puzzling behavior will be investigated in ongoing experiments.
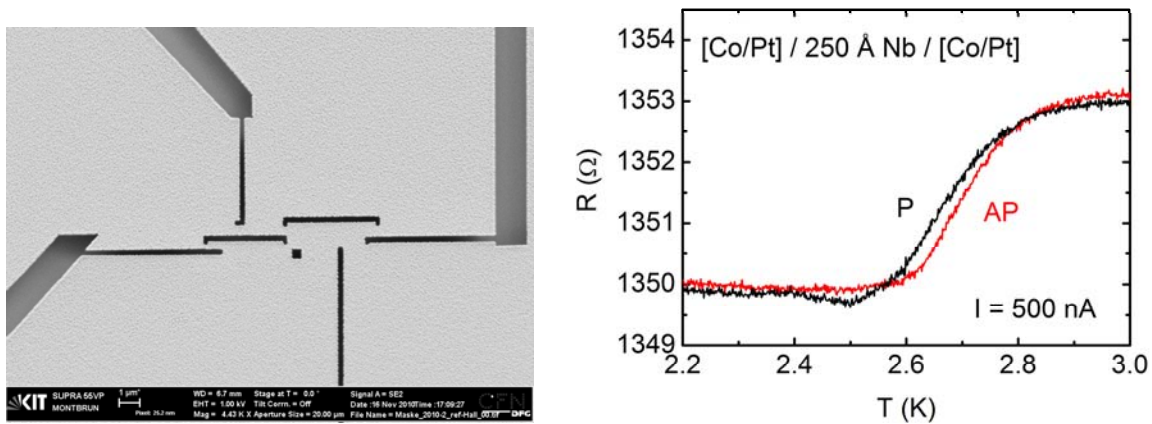

Fig. 5: Left: Electronmicrograph of an underetched Si_3N_4 mask on SiO_2/Si for shadow evaporation of F/S/F hybrid structures (image width 25 μm). Right: Supercondcutive transition of a [Co/Pt]/Nb/[Co/Pt] structures with current perpendicular to the plane in the parallel (P) and antiparallel (AP) state.

3. Determination of the Current Spin Polarization in S/F Point Contacts

The proximity effect is mediated by the microscopic process of Andreev reflection (AR) at the S/F interface by which an incident electron from N or F is retro-reflected as a hole, thus creating a Cooper pair in S. The sensitivity of the Andreev process to the spin of the carriers originates from the spin content of a Cooper pair (S = 0 in conventional superconductors) and the conservation of the spin direction at the interface. This spin sensitivity of the AR is utilized to determine the degree of the current spin-polarization P by point-contact spectroscopy between S and F [12]. P is an important ingredient in technological applications where the information is written by driving a spin-polarized current through a spin-sensitive memory. The analysis of Andreev reflection in superconductor/ferromagnet (S/F) point contacts has been used to extract the spin polarization P in a great variety of materials by various groups. The theoretical analysis of these S/F point-contact (PC) experiments has been mainly carried out using a generalization of the Blonder-Tinkham-Klapwijk (BTK) theory [13], where the AR current is decomposed into a fully spin-polarized and fully unpolarized current. However, these extended BTK models are not microscopically justified and the fitted parameters are usually temperature dependent.
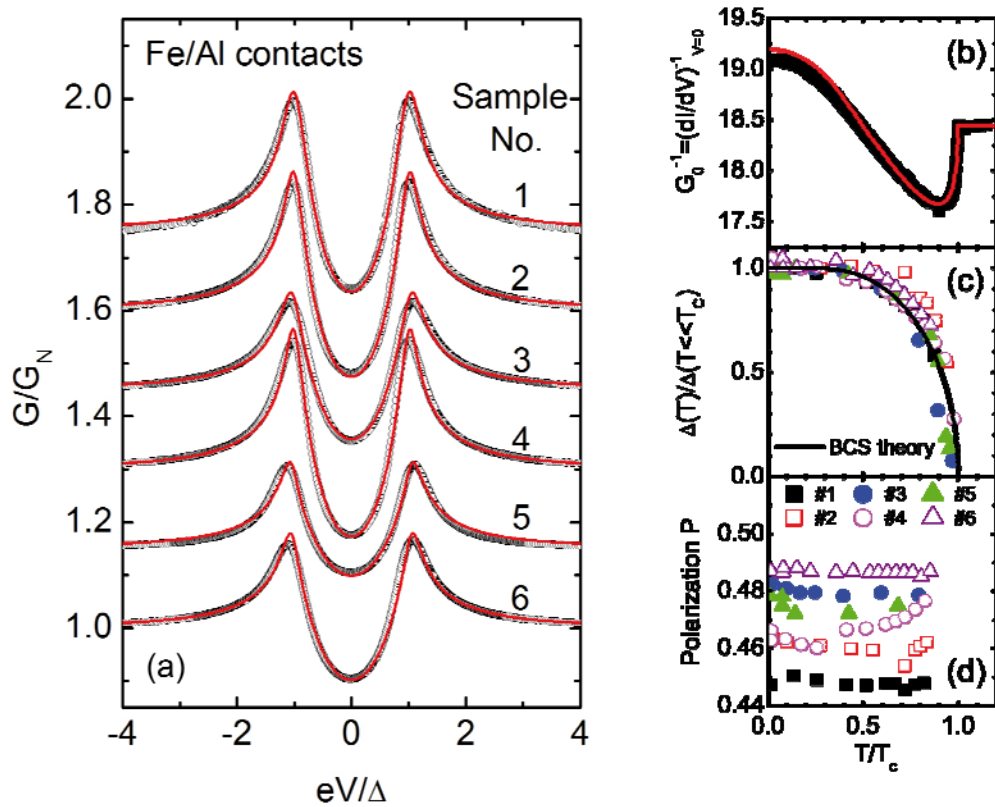

Fig. 6: (a) Andreev spectra of Al/Fe nanocontacts. For clarity, the curves are shifted successively upward. The solid lines are the calculated spectra with our model. (b) T dependence of the zero-bias resistance G_0^{-1} together with a theoretical curve (red). (c) T dependence of the superconducting gap Δ for all investigated samples, obtained from a least-squares fit of the data and normalized to Δ ($T = 200$ mK $\ll T_c$). (d) T dependence of the current spin polarization P. From Ref. [B2.7:12].

In collaboration with the theory group in project B2.6 we have developed a microscopic model of the spin-dependent transport in S/F contacts with two spin-dependent transmission coefficients $\tau_\uparrow$ and $\tau_\downarrow$ [14] for transport across the F/S interface. These coefficients contain the relevant microscopic properties. This $\tau_\uparrow$-$\tau_\downarrow$ model has been used to analyze PC spectra of Al/Co, Al/Fe, and In/Ni contacts [14,15, B2.7:12]. Nanostructured Al/F (F = Co, Fe) point contacts have been fabricated [14, B2.7:12] following the process described in Ref. [16]. Using $\tau_\uparrow$, $\tau_\downarrow$, and the superconductive energy gap Δ as free parameters our model yields an excellent fit to the Andreev spectra of the Al/Co contacts for temperatures $T \approx$ 100 mK [14] and for Al/Fe contacts, see Fig. 6(a). The model also describes without any additional fit parameter the temperature and magnetic-field dependence of the conductance (not shown) [14].

The high stability of nanostructured PCs, together with the high quality of the fits, allows a detailed investigation of the T dependence of $\Delta(T)$ and $P(T)$. $\Delta(T)$ follows the standard BCS dependence, Fig. 6(c) (solid line). The current spin polarization P for each sample is independent of T within the error of the least-squares fitting procedure, Fig. 6(d). This strongly supports our assignment of P as an intrinsic parameter of the particular S/F point contact under study. Indeed, P depends on R_N in a systematic fashion; i.e., larger contact resistances go along with larger P. The radius a of a circular homocontact can be calculated from R_N for different regimes of current flow through the contact, depending on the ratio of a to the electron mean free path l of the material [17]. $P(a)$ decreases systematically as displayed in Fig. 7.
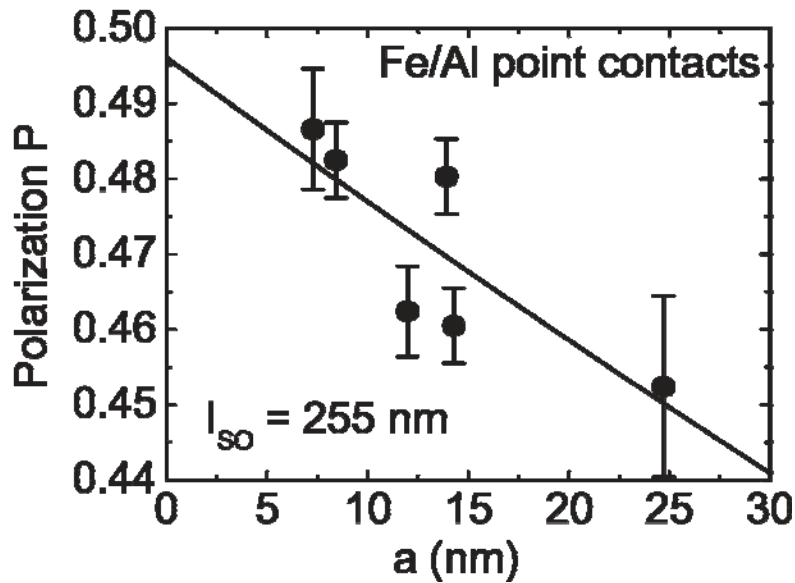

Fig. 7: Dependence of the current spin polarization on the contact radius. Solid line shows $P = P_0 \exp(-a/l_{so})$ with $P_0 = 0.496 \pm 0.01$ and $l_{so} = 255 \pm 91$ nm. From Ref. [B2.7:12].

A possible explanation of the $P(a)$ dependence is as follows. For large a, the incident electrons probe a larger volume before being retroreflected as a hole than for a small a. Any scattering process affecting P will therefore have a stronger effect for larger contacts [17]. We suggest that spin-orbit scattering — with a constant scattering length — is operative as the main source of the reduction of P and model the dependence $P(a)$ by a simple exponential decay. We obtain a spin-orbit scattering length $l_{so} = 255 \pm 91$ nm from a fit to the data in Fig. 7. This value is very

reasonable albeit somewhat lower than the spin diffusion length l_{sd} = 500 - 1000 nm found for Al [18], which may be attributed to a smaller elastic mean free path of our Al films or minor interdiffusion at the Al/Fe interface. With this interpretation, our data constitute a clear relation between the spin polarization of the Andreev current and the bulk spin polarization.

4. Non-local Andreev Reflection in Superconductor Hybrid Structures

We have investigated non-local transport in multiterminal superconductor hybrid structures. These structures consist of a superconducting (S) aluminum wire of about 150 nm width and 15-30 nm thickness. Two or more non-magnetic copper (N) or ferromagnetic iron (F) wires are in contact to the aluminum wire at distances ranging from 100 nm to several μm. Prior to depositing the normal metal, the aluminum is oxidized weakly to form an ultra-thin insulating (I) oxide tunnel barrier.
In the multiterminal geometry used here, non-local effects not observable in single contacts occur: An electron injected into the superconductor from one electrode may be reflected as a hole into a nearby detector electrode, rather than into the same. This process is called crossed Andreev reflection (CAR).
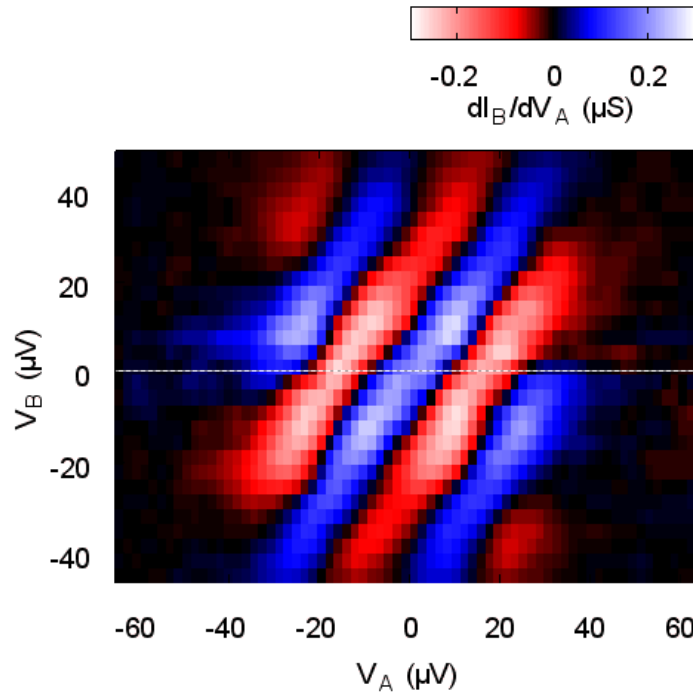

Fig. 8: Non-local subgap conductance pattern due to CAR and EC. From Ref. [B2.7:15].

CAR competes with other non-local transport processes. An electron entering a superconductor at energies below the energy gap can only occupy a virtual state for a short time. This opens the possibility for a cotunneling event, where an electron leaves the superconductor through the second (detector) electrode (elastic cotunneling, EC). A third competing transport mechanism is charge imbalance (CI) due to injection above the energy gap. We have performed detailed investigations of CAR, EC and CI in NISIN and FISIF structures. In FISIF structures, a negative four-terminal resistance due to CAR was observed [B2.7:4]. In NISIN structures, we have found a competition of CAR and EC at subgap energies, with a complex dependence on the bias voltages applied to both injector and detector contact [B2.7:15], see Fig. 8. These non-local phenomena were found to be

linked to an anomaly in the local conductance, which is probably caused by quantum-mechanical interference (reflectionless tunneling).
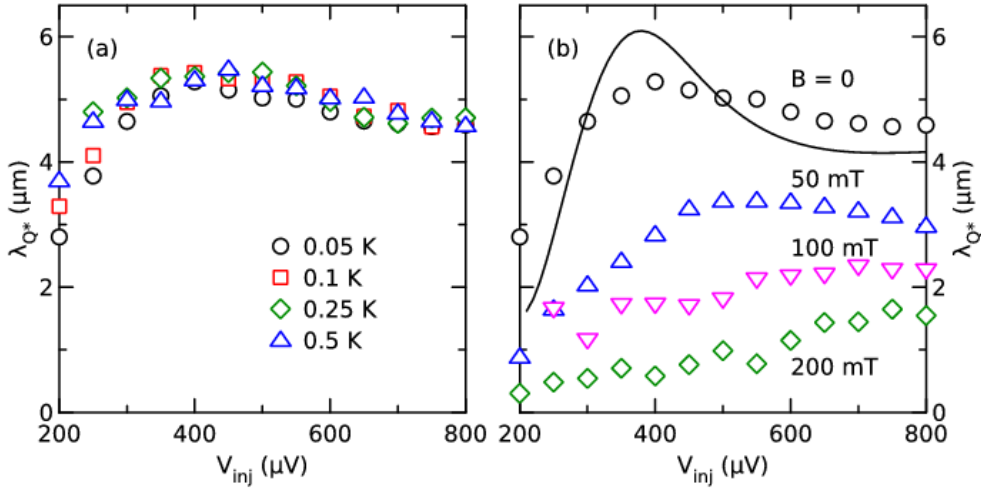

Fig. 9: Charge-imbalance relaxation length as a function of temperature and magnetic field. From Ref. [B2.7:14].

We have also measured non-local charge imbalance at ultra-low temperatures as a function of bias, contact distance, temperature, and magnetic field [B2.7:14], see Fig. 9. These results allow us to distinguish unambigiously coherent subgap transport due to CAR and EC from CI.

5. Electronic Transport in Pd films on $Eu_xSr_{1-x}S$

Among the elemental transition metals, palladium takes a unique position. It is very close to a ferromagnetic instability because of the large electronic density of states at the Fermi level and a large Stoner enhancement factor. Minute additions of Fe render Pd ferromagnetic, with a critical concentration $x_c \approx 0.01$ at% [19]. Moreover, Pd may become ferromagnetic in thin films or nanoparticles due to the expansion of the crystalline lattice. On the other hand, Pd is very susceptible to superconductivity induced by minor modifications of the electron density or electronic structure. In all these instances, superconductivity is believed to be conventional, i.e., mediated by electron-phonon coupling leading to an s-wave order parameter. In contrast, p-wave superconductivity was predicted for Pd [20] but until now has not been observed, possibly due to pair breaking by nonmagnetic impurities [21].

We have investigated the electronic transport properties of very thin Pd films in contact to a magnetically ordered substrate. We have chosen $Eu_xSr_{1-x}S$, a magnetic semiconductor allowing tuning of the magnetic properties by variation of the Eu concentration x from nonmagnetic ($x = 0$) via spin-glass to ferromagnetic ($x = 1$) [22]. Pd of thickness $d_{Pd} = 7 - 30$ nm was deposited onto an epitaxially grown $Eu_xSr_{1-x}S$ film. Surprisingly, very thin Pd films $Eu_xSr_{1-x}S$ are superconducting below 1 K. Figure 11 shows the sheet resistance $R_\square(T)$ in the low temperature regions for 7-nm Pd films on (a) SrS (a), and on (b) $Eu_{0.55}Sr_{0.45}S$ in perpendicular magnetic fields. In zero field, superconducting transitions at $T_c = 0.9$ K ($x = 0$) and $T_c = 0.67$ K ($x = 0.55$) are observed. From the

resistive T_c measured in magnetic fields, we determine the upper critical fields B_{c2} and estimate the BCS coherence length $\xi_0 = 93$ nm (dirty limit) for the superconducting Pd film on SrS.

We observed superconductivity in $R_\square$ (T) for Pd films on $Eu_xSr_{1-x}S$ with other Eu concentrations as well, except for $x = 1$. Fig. 11(a) shows that $T_c(x)$ decreases monotonically with increasing x. The reduction of T_c is likely due to magnetic pair breaking by contact of Pd with the ferromagnetic semiconductor. The pair breaking by magnetic Eu^{2+} ions suggests immediately that the observed superconductivity in Pd films is s-wave.
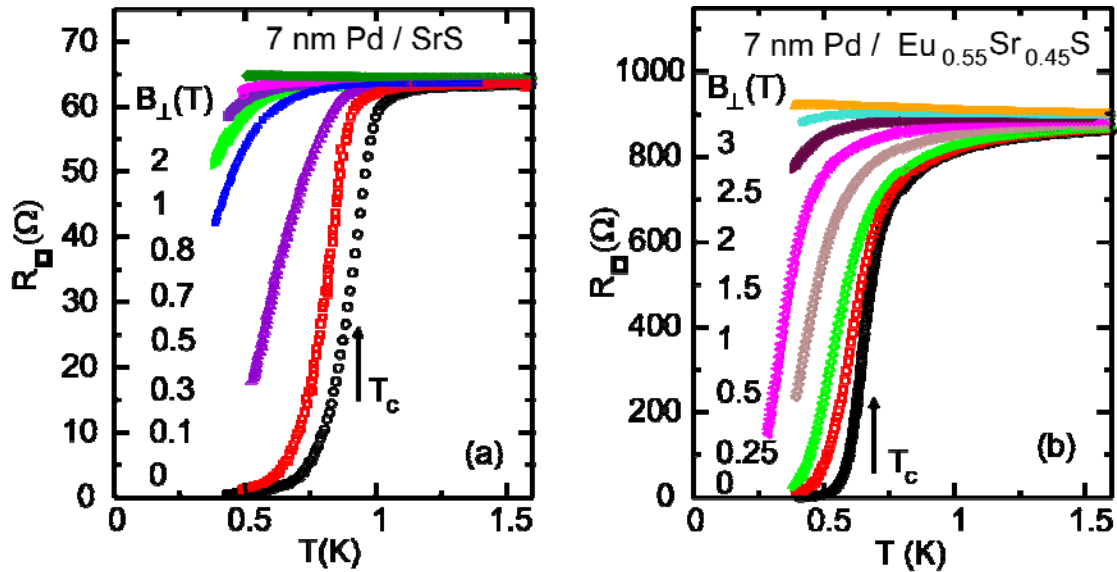

Fig 10: Resistance $R(T)$ of a 7-nm Pd film on (a) SrS and on (b) $Eu_{0.6}Sr_{0.4}S$ for different perpendicular magnetic fields B.

The reduction of T_c by pair-breaking processes such as magnetic fields or magnetic impurities is usually characterized by the pair-breaking parameter α in the Abrikosov-Gor'kov (AG) theory [23]. Fig. 11(b) shows the reduced transition temperatures $t = T_c/T_{c0}$ vs. T_C/T_{C0} of all samples together with the universal behavior obtained from the AG theory assuming that $\alpha \sim T_C/T_{C0}$. T_{c0} and T_{C0} are the superconductive transition temperature and Curie temperature, respectively, for the sample with $x = 0$. A more adequate description for the present case of a magnetic insulator was given by Tokuyasu, Sauls, and Rainer (TSR) [24] who considered a thin superconducting film of thickness $d < \xi_0$ sandwiched between a magnetic and a nonmagnetic insulator. The spins of quasiparticles impinging on and reflected from the superconductor/magnet interface are rotated by the spin-mixing angle θ. This magnetic scattering at the magnetic interface destroys superconductivity even for $\theta \ll 1$ [24]. In general, θ depends on the projection of the spin on the surface normal to every trajectory. The reduced superconductive transition temperature decreases with increasing pair-breaking parameter α_{TSR}, where $\alpha_{TSR} = \xi_0 \tan(\theta/2)/2d$. For $\alpha_{TSR} = \alpha_{TSR,c} = 0.3816$, superconductivity is completely suppressed $(t = 0)$. Fig. 11(b) shows t vs. a_{TSR} (dashed-dotted line) taken from Ref. [24]. For the values of ξ_0 and d of our superconducting film $\alpha_{TSR} \sim \theta$ would be expected which is at variance with our data, if we assume that the spin-mixing angle scales linearly with the Curie temperature. An obvious explanation is that the assumption $\theta \sim T_C$ may be incorrect. The nonlinearity of $\theta(T_C/T_{C0})$ calculated from the measured t [24] might reflect a different spin-mixing

angle at a superconductor/spin-glass compared to a superconductor/ferromagnet interface, with an apparently stronger pair breaking by the spin-glass than by the ferromagnet.
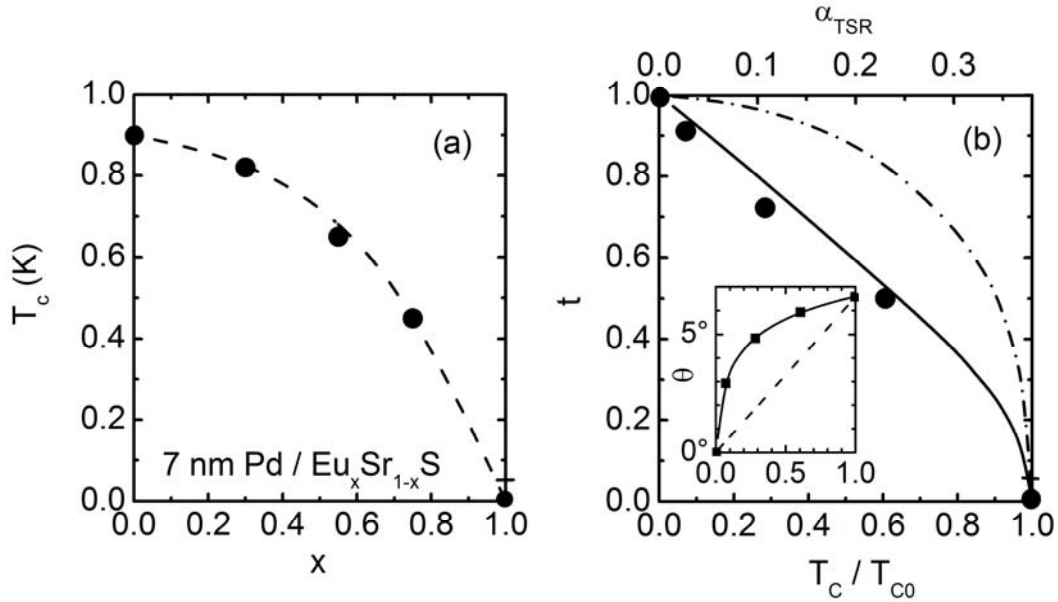
Fig. 11 (a) $T_c(x)$ of 7 nm Pd on $Eu_xSr_{1-x}S$. Dashed line serves as guide to the eye. For $x = 1$, no superconducting transition was found down to 50 mK. (b) Scaled superconductive transition temperature t vs. scaled Curie temperature T_C/T_{C0}. Solid line shows the universal functional behavior obtained from the Abrikosov-Gor'kov theory for a pair-breaking parameter α_{AG} taken as the reduced Curie temperature T_C/T_{C0}. Dashed-dotted curve represents the theoretical $t(\alpha_{TSR})$ dependence due to pair breaking by the proximity of superconducting Pd to an insulating ferromagnet [24]. Inset shows the spin-mixing angle θ vs. T_C/T_{C0}. Dashed line shows a linear dependence $\theta(T_C/T_{C0})$ expected from the theoretical $t(\alpha_{TSR})$ curve.

Possible origins of superconductivity we suggest to arise from electron charge transfer reducing the density of states at the Fermi level. Indeed, we have observed a decrease of the resistance jump at T_c upon applying a positive gate voltage to the Pd film (not shown). Negative gate voltages, on the other hand, did not alter the superconducting transition. Thus, a negative charge transfer from Pd to the $Eu_xSr_{1-x}S$ substrate may indeed be responsible for superconductivity. In line with this argument, we observe a positive Hall coefficient for our superconducting films. Two possibilities for the cause of the charge transfer remain: (1) strongly electronegative sulfur at the interface ``binding'' electrons and (2) formation of an interfacial Pd-S layer of unknown stoichiometry. In both cases, we expect superconductivity to be stable in only a small window of thickness, because for larger thickness the nonsuperconducting portion of the Pd film would suppress superconductivity in the thin layer adjacent to the $Eu_xSr_{1-x}S$ surface. In conclusion, our surprising observation of superconductivity in very thin Pd films of 7 nm thickness deposited on $Eu_xSr_{1-x}S$ ($0 \leq x < 1$) indicates an appreciable charge transfer at the interface. This is quite unusual for a metallic system with high conduction-electron density.

References

- own work with complete titles -

[1] A. I. Buzdin, Rev. Mod. Phys. **77** (2005) 935

[2] A. L. Fauchère and G. Blatter, Phys. Rev. B **56**, 14102 (1997)

[3] L. R. Tagirov, Phys. Rev. Lett. **83**, 2058 (1999)

[4] J. Y. Gu, C. Y. You, J.S. Jiang, J. Pearson, Ya. B. Bazaliy, S.D. Bader: Phys. Rev. Lett. **89**, 267001 (2002)

[5] R. Steiner and P. Ziemann, Phys. Rev. B **74,** 094504 (2006)

[6] V. Peña, Z. Sefrioui, D. Arias, C. Leon, J. Santamaria, J. L. Martinez, S. G. E. te Velthuis, A. Hoffmann, Phys. Rev. Lett. **94**, 057002 (2005)

[7] W. Gillijns, A. Yu. Aladyshkin, M. Lange, M. J. Van Bael, V. V. Moshchalkov, Phys. Rev. Lett. **95,** 227003 (2005)

[8] I. C. Moraru, W. P. Pratt, Jr., N. O. Birge, Phys. Rev. Lett. **96**, 037004 (2006)

[9] A. I. Buzdin, A. V. Vedyayev, and N. V. Ryzhanova, Europhys. Lett. **48**, 686 (1999)

[10] T. Yamashita, S. Maekawa, Phys. Rev. B **67**, 094515 (2003)

[11] C. Sürgers, T. Hoss, C. Schönenberger, C. Strunk: *Fabrication and superconducting properties of nanostructured SFS contacts*, J. Magn. Magn. Mat. **240**, 598 (2002)

[12] M. J. M. de Jong,C. W. J. Beenakker, Phys.Rev.Lett. **74**1657 (1995)

[13] G. E. Blonder, M. Tinkham, T.M. Klapwijk, Phys. Rev. B **25** 4515 (1982)

[14] F. Pérez-Willard, J.C. Cuevas, P. Pfundstein, J. Kopu, M. Eschrig, C. Sürgers, H. v. Löhneysen: *Determining the spin-polarized current through Al/Co nanostructured point contacts*, Phys. Rev. B **69**, 140502(R) (2004)

[15] S. Hacohen-Gourgy, B. Almog, G. Deutscher, Appl. Phys. Lett. **92**, 152502 (2008)

[16] K. S. Ralls, R. A. Buhrman, R. C. Tiberio, Appl. Phys. Lett. **55**, 2459 (1989)

[17] Y. Naidyuk and I.K. Yanson: Point Contact Spectroscopy (Springer, Berlin, 2004)

[18] D. Beckmann, H.B. Weber, H. v. Löhneysen: *Evidence for crossed Andreev reflection in superconductor-ferromagnet hybrid structures,* Phys. Rev. Lett. **93**, 197003 (2004)

[19] C. Büscher, T. Auerswald, E. Scheer, A. Schröder, H. v. Löhneysen, H. Claus: *Ferromagnetic transition in dilute Pd-Fe alloys*, Phys. Rev. B **46**, 983 (1992)

[20] D. Fay and J. Appel, Phys. Rev. B **16**, 2325 (1977)

[21] F. Pobell, Physica **109-100 B**, 1485 (1982)

[22] H. Maletta and W. Felsch, Z. Phys. B **37**, 55 (1980)

[23] A. A. Abrikosov and L. P. Gor'kov, Sov. Phys. JETP **12**, 1243 (1961)

[24] T. Tokuyasu, J. A. Sauls, D. Rainer, Phys. Rev. B **38**, 8823 (1988)